Electron Transfer Inside a Decaferrocenylated Rotaxane Analyzed by Fast Scan Cyclic Voltammetry and Impedance Spectroscopy

Gabriel Boitel-Aullen, Laure F Fillaud, François Huet, Iwona Nierengarten, Béatrice Delavaux-Nicot, Jean-François Nierengarten, Emmanuel Maisonhaute

Electron Transfer Inside a Decaferrocenylated Rotaxane Analyzed by Fast Scan Cyclic Voltammetry and Impedance Spectroscopy.

Gabriel Boitel-Aullen,[a] Laure Fillaud,[a] François Huet,[a] Iwona Nierengarten,[b] Béatrice Delavaux-Nicot,[c] Jean-François Nierengarten,*[b] and Emmanuel Maisonhaute*[a]

In memory of Professor J.-M. Savéant

[a] Mr. G. Boitel-Aullen, Dr. L. Fillaud, Pr. F. Huet, Pr. E. Maisonhaute
Sorbonne Université, CNRS, Laboratoire Interfaces et Systèmes Electrochimiques, 4 place Jussieu, 75005 Paris, France
E-mail: emmanuel.maisonhaute@sorbonne-universite.fr

[b] Dr. I. Nierengarten, Dr. J.-F. Nierengarten
Laboratoire de Chimie des Matériaux Moléculaires,
Université de Strasbourg et CNRS (LIMA – UMR 7042), Ecole Européenne de Chimie, Polymères et Matériaux (ECPM)
25 rue Becquerel, 67087 Strasbourg Cedex 2 (France)
E-mail: nierengarten@unistra.fr

[c] Dr. B. Delavaux-Nicot
Laboratoire de Chimie de Coordination du CNRS (UPR 8241)
Université de Toulouse (UPS, INPT)
205 route de Narbonne
BP 44099, F-31077 Toulouse Cedex 4, France.

Supporting information for this article is given via a link at the end of the document.

Abstract: The electrochemical behavior of a giant rotaxane bearing 10 electroactive ferrocene centers has been analyzed by both fast scan cyclic voltammetry and impedance measurements. The measurements support the hypothesis that all redox centers are not equivalent and display different electron transfer rate constants, which would arise from several possible conformations of the adsorbed molecule. Effectively using such systems in molecular devices thus necessitates to minimize or at least control those dispersions.

Introduction

Approaches such as those developed by Jean-Michel Savéant and his school greatly contributed to the understanding of electron transfer mechanisms inside complex systems. Those may be revealed by following specific observables such as peak potential or current in cyclic voltammetry (CV).[1] Deviations from this general framework often reveal interactions or heterogeneities of the system, as may be observed with modified electrodes. For example, it has been recognized from a long time that even if self-assembly of thiolated systems onto gold surfaces produces very rapidly (within minutes) a large coverage, obtaining reproducible results necessitates long immersion times (usually one night).[2–5] Molecule/surface interactions and ordering indeed resort to many dynamic processes that cover multiple timescales, and reaching equilibrium may take up to a few days.[3–6] For ideal isolated redox centers that transfer a single electron, the CV peak should present a symmetric bell-shape with a full width at half maximum of 91 mV at room temperature.[1,7,8] This behavior is however seldom observed even within self-assembled monolayers (SAMs) of rather simple systems because redox centers may interact together or with their matrix. Many interesting models have been proposed to take these interactions into account and also sometimes include kinetic aspects. For example, Laviron considered Frumkin isotherms[9] while Smith et al. calculated the influence of electrostatic interactions.[10] More recently, Levillain et al. proposed a generalized interaction model that can take into account random or non-random distribution of electroactive centers.[11–15] In all cases, the response tends towards ideality when the surfacic concentration decreases. Nevertheless, despite the care in electrode preparation, monolayers are sometimes not uniform, and present defects such as pinholes[16] or distribution of different environments or distances from the electrode for the redox centers.[17] Those may translate in distributions of apparent standard potentials E^0 and kinetic rate constants $k_{ET}{}^0$ as examined initially by Albery and then by Murray for self-assembed monolayers.[18,19] Disentangling all effects benefits from analyzing the systems with a range of techniques. In this paper, we have examined in details the kinetic dispersion of the decaferrocenylated rotaxane **1** presented in Figure **1** adsorbed onto a gold ultramicroelectrode. Rotaxanes represent a new avenue in supramolecular chemistry since they offer the possibility to tailor either the axle or the macrocyclic ring with many functions, in particular redox centers.[20] A wide field of potential applications are concerned, such as molecular electronics,[21] sensing[22] or artificial muscles[23–25] for example. Those systems allow to propagate an electrochemical perturbation over long distances through electron hopping from the ferrocene layer close to the electrode towards centers positioned at larger distances from the electrode. Practical applications require fast signal transduction, which translates into the necessity to develop adequate instrumentation and methodologies.[26–32] The synthesis, surface modification procedure and CV characterization of molecule **1** were already examined earlier,[33] It was demonstrated with fast scan CV that hopping within this structure is extremely fast and then transparent in the measurements. Here we will focus on the

complementarity of CV and impedance measurements using high frequencies to analyze slight kinetic deviations from ideality.

Figure 1. Molecule **1** presents 10 ferrocene units that display ultrafast electron

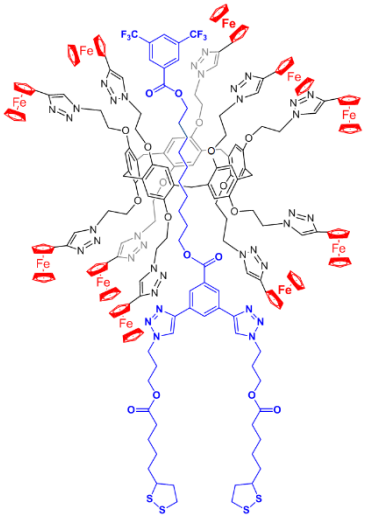

transfer with the gold electrode onto which it is anchored.

Results and Discussion

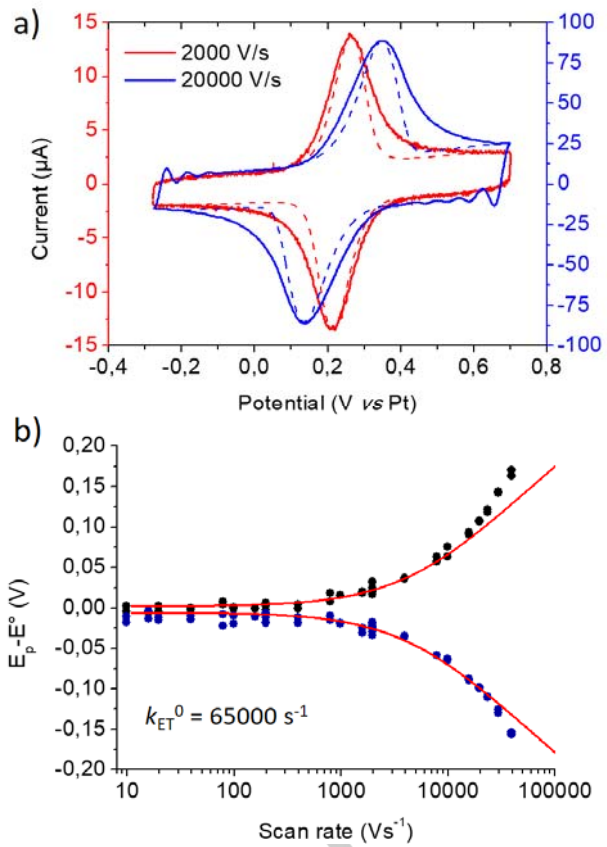

Figure 2. a) Cyclic voltammograms at 2000 (red) and 20000 Vs^{-1} (blue) of molecule **1** adsorbed on a gold microelectrode recorded in acetonitrile + 0.50 M tetrabutylammonium hexafluorophosphate. Dashed lines: fits with k_{ET}^0 = 65000 s^{-1}, α = 0.5 using Butler-Volmer theory. b) Dots: Trumpet plots recording the forward (black) and backward (blue) peak potentials at different scan rates. Red lines: theoretical variations according to Butler-Volmer theory with a predominant rate constant of k_{ET}^0 = 65000 s^{-1}.

Figure 2 presents a typical CV at 2000 Vs^{-1} acquired in acetonitrile + 0.50 M tetrabutylammonium hexafluorophosphate for **1** adsorbed onto a 10400 µm^2 gold ultramicroelectrode during 48 hours. In this low scan rate regime, the peaks present a bell-shape with a mean peak potential value of +0.239 ± 0.003 V *vs* Pt. At 20000 Vs^{-1}, the oscillations at the potential inversions are due to ohmic drop compensation that is necessary to obtain reliable data. The molecular coverage is estimated by integration of oxidation and reduction peaks at Γ^0 = 98 ± 3 nmolm^{-2}. Thus each molecule occupies in average an area of 17.0 ± 0.4 nm^2, confirming formation of a monolayer. The peak to peak potential difference at low scan rate is only 8 mV, very close to the theoretical one of 0 mV for ideal Nernstian systems.[1,9] At 20000 Vs^{-1}, the peaks shift from equilibrium position because the characteristic time scale of the voltammetry becomes comparable to the electron transfer one. CVs in the range 10-40000 Vs^{-1} are provided in Figure S1, and the corresponding peak potentials are reported in Figure 2b in the so-called "trumpet plots".[9] Their fit with Butler-Volmer theory provides an average rate constant k_{ET}^0 = 65000 ± 5000 s^{-1} at $E = E^0$. The apparent disagreement at scan rates above 20000 Vs^{-1} is purely instrumental and caused by the bandwidth limitation of the electrochemical equipment. Nevertheless, simulation of the oxidation and reduction peaks as displayed in Figure 2 (dashed lines) reveals that the peak width is larger than the theoretical one, and that this deviation is more apparent at large scan rates. Indeed, at 20000 Vs^{-1}, a full-width at half maximum of 178 ± 4 mV was found, whereas theoretical values expected from Butler-Volmer (BV) and Marcus-Hush-Chidsey (MHC) theories are of 120 mV and 129 mV, respectively. In fact, MHC theory is more accurate and physically significant than Butler-Volmer one.[27,34–36] In this framework, at large overpotentials k_{ET} departs from its intrinsic exponential dependence with the electrode potential to potentially level out. This translates as broader CV shapes.[36–39] However, here overpotentials of less than 100 mV are concerned until 20000 Vs^{-1}, so that the larger full width at half maximum cannot be attributed to Marcus-Hush-Chidsey effects. These effects may only explain the small "tail" in the peak as confirmed by the numerical simulations presented in Figure S2.

We underline that such deviations remain tiny and are frequently observed for adsorbed systems. Considering that the density of redox centers is low and that a large supporting electrolyte concentration is used, we will below neglect their interactions even if we are aware that this may be an oversimplification.[14] In the following, in order to examine more deeply the origin of this slight discrepancy, we complement the CV results with impedance ones performed onto exactly the same modified electrode and under the same conditions.

Indeed, impedance provides the possibility to examine the behavior of a system at a given potential and is thus complementary to cyclic voltammetry.[40] For that, it is necessary that the system does not degrade, which limits the potential excursion. To check the SAM integrity, a control cyclic voltammogram was performed after each impedance spectrum acquisition. We observed that the surface coverage did not decrease by more than 5% compared to the one measured at the beginning of the experiment.

Electrochemical impedance spectroscopy has been less used than cyclic voltammetry in molecular electrochemistry though Savéant et al. punctually demonstrated its interest.[41,42] For self-assembled monolayers, Creager et al. proposed in 1998

impedance as an alternative method to assess electron transfer rates within self-assembled monolayers.[14,43–45] Here, the electrode is polarized at a potential E_m, onto which is added a small sinusoidal perturbation of amplitude ΔE, so that:

$$E = E_m + \Delta E e^{j\omega t} \qquad (1)$$

with ω the angular frequency. The authors relied on the equivalent electrical model enclosed in the red box in Scheme 1a and we recall below the main formulations and conclusions.

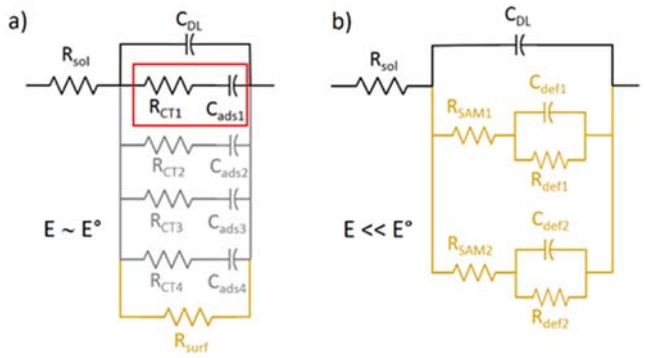

Scheme 1. Electrical equivalent schemes of the electrochemical cell. R_{sol}: solution resistance. C_{DL}: double layer capacitance. a) At $E \sim E^0$ several populations Γ_i^0 of electron transfer rate constants k_{ETi}^0 may contribute to the signal through different R_{CTi} and C_{adsi}. These elements are absent at $E << E^0$ in (b). Deviations at low frequencies are taken into account by additional high impedance elements represented in yellow (see text).

In this model, the complex impedance Z of the system may be expressed as:

$$\frac{1}{Z} = \frac{n(j\omega)\Gamma^0 k_{ET}^0 F^2 S}{RT} \frac{e^{\frac{-\alpha F(E_m-E^\circ)}{RT}}}{\left(1+e^{\frac{-F(E_m-E^\circ)}{RT}}\right)\left(j\omega+k_{ET}^0 e^{\frac{-\alpha F(E_m-E^\circ)}{RT}}\left(1+e^{\frac{F(E_m-E^\circ)}{RT}}\right)\right)} \qquad (2)$$

Where Γ^0 is the density of molecules having n redox sites transferring electrons at the rate constant k_{ET}^0 onto the electrode of surface S (α is the charge transfer coefficient taken as 0.5 in all this study, R = 8.314 $JK^{-1}mol^{-1}$, F = 96485 $C.mol^{-1}$ and T = 293 K). At low frequencies, faradaic processes are at equilibrium with the electrode potential and can thus be modeled with a potential-dependent capacitance proportional to the surface coverage:

$$C_{ads} = \frac{n\Gamma^0 F^2 S}{RT} \frac{e^{\frac{F(E_m-E^\circ)}{RT}}}{\left(1+e^{\frac{F(E_m-E^\circ)}{RT}}\right)^2} \qquad (3)$$

At very high frequencies, charge transfer kinetics interferes, and for $k_{ET}^0 << \omega$ the system is purely resistive, the charge transfer resistance R_{CT} being expressed as:

$$R_{CT} = \frac{RT}{n\Gamma^0 k_{ET}^0 F^2 S} \frac{\left(1+e^{\frac{-F(E_m-E^\circ)}{RT}}\right)}{e^{\frac{-\alpha F(E_m-E^\circ)}{RT}}} \qquad (4)$$

One can notice that when the electrode is polarized at the standard potential of the redox process, that is, if $E_m = E^\circ$, equation (3) reduces to equation (5), and the rate constant k_{ET}^0 can be determined with equation (6):

$$C_{ads}^0 = \frac{n\Gamma^0 F^2 S}{4RT} \qquad (5) \qquad k_{ET}^0 = \frac{1}{2R_{CT}C_{ads}} \qquad (6)$$

For real systems that display heterogeneities, capacitances are often replaced by a constant phase element (CPE) so that:

$$Z_{CPE} = \frac{1}{Q_{CPE}(j\omega)^\varphi} \qquad (7)$$

The parameter φ ($0 \le \varphi \le 1$) reflects the heterogeneities.[40] When $\varphi = 1$, Q_{CPE} is a pure capacitance, and conversely when $\varphi = 0$, Z_{CPE} is a pure resistance.
In practice, one has to handle also the solution resistance R_{sol} and double layer capacitance C_{DL} so that the global equivalent impedance for an ideal system is now expressed as:

$$Z = \frac{1+j\omega(R_{CT}C_{ads}+R_{sol}C_{ads}+R_{sol}C_{DL})-\omega^2 R_{sol}C_{DL}R_{CT}C_{ads}}{j\omega(C_{ads}+C_{DL})-\omega^2 R_{CT}C_{DL}C_{ads}} \qquad (8)$$

This formulation demonstrates that at low frequencies or equivalently for Nernstian systems, the impedance is purely capacitive, being the sum of the adsorption and double layer capacitance. Hence impedance will be sensitive to adsorbed centers only provided that they are in sufficient number so that C_{ads} is not negligible compared to C_{DL}. At very high frequencies the response is dominated by the electrolyte resistance as usual in any impedance measurement. Therefore, the impedance is sensitive to the electron transfer kinetics only provided that the quantity $R_{CT}C_{ads}$ is non negligible compared to $R_{sol}C_{ads}$ and $R_{sol}C_{DL}$ as detailed further in SI.
These conclusions are reminiscent from those encountered in fast scan cyclic voltammetry for which one has to fulfill $k_{ET}^0 \sim 1/R_{sol}C_{DL}$ to observe a significant peak shift. One difference however is that in CV, Γ^0 only plays a role in the signal/noise resolution since the peak current is itself proportional to Γ^0 but does not appear directly in the kinetic measurements. Conversely, it plays a major role in impedance through the term C_{ads} which is important also in signal/noise resolution but also for kinetic determination through the term $R_{CT}C_{ads}$.
Whereas Creager et al. chose some frequencies and recorded the impedance in the so-called AC voltammetry configuration, we wished to avoid polarization of the electrode at oxidative potentials for a too long time to prevent SAM degradation.[14,43] We thus investigated a modified electrode by impedance spectroscopy in the frequency range 10^2 -10^7 Hz at fixed potentials. Figure 3 presents the results obtained at two potentials for the same electrode. We chose two complementary representations to interpret and fit our data. In the first one impedance modulus and phase are represented as a function of frequency in the classical Bode plots. In the second one, proposed by Bueno et al.,[46–48] the so-called complex capacitance C^* is calculated with equation (9):

$$C^* = C' + jC'' = \frac{1}{Zj\omega} \qquad (9)$$

The real (*C*') and imaginary (*C*" or -*C*") capacitances can thus be represented in semi-log plots as a function of frequency. Alternatively, -*C*" versus *C*' Nyquist plots are provided in SI. The advantage of such approach is to provide a convenient visualization of data over a large range of frequencies.

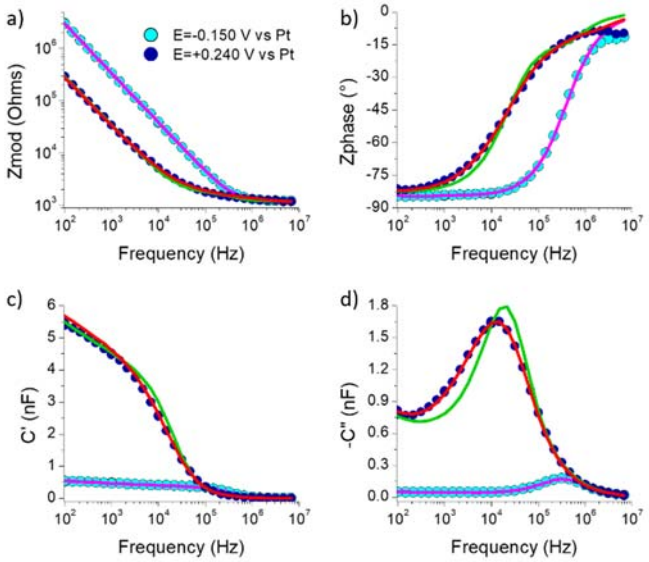

Figure 3. Analysis of impedance data acquired at E_m = -0.150 V *vs* Pt << E^0 (cyan dots) and E_m = +0.240 V vs Pt = E^0 (blue dots) onto a gold ball ultramicroelectrode with an area of 10400 µm². Pink line: simulation without faradaic process. Green line: simulations with a single faradaic process (R_{CT} = 908 Ω ; C_{ads} = 8.01 nF, φ = 0.912) ; R_{sol} = 1190 Ω ; C_{DL} = 1.27 nF, φ_{DL} = 0.948). Red line: simulations with 4 populations, each having its own R_{CTi} and C_{adsi} value (R_{CT1} = 77700 Ω ; C_{ads1} = 1.64 nF, φ_1 = 0.891 ; R_{CT2} = 12000 Ω ; C_{ads2} = 1.84 nF, φ_2 = 0.940 ; R_{CT3} = 1870 Ω ; C_{ads3} = 2.79 nF, φ_3 = 0.938 ; R_{CT4} = 758 Ω ; C_{ads4} = 1.69 nF, φ_4 = 0.916 ; R_{sol} = 1190 Ω ; C_{DL} = 1.18 nF, φ_{DL} = 0.947). a) Impedance b) Phase. c) Real capacitance C' d) Imaginary capacitance - C".

At $E << E^0$ (cf. Figure 3, cyan dots, see also Figure S3-S6) C_{ads} = 0. The response is dominated by the R_{sol} and C_{DL} components which is translated into a peak in the –C" component at $\omega \simeq R_{sol}C_{DL}$ (see SI for the analytical formulation). However, as observed for other self-assembled monolayers, the phase does not reach -90° for low frequencies as should be expected for a pure RC system (cf. Figure 3b). This is attributed to ion permeation into the layer, a potential-dependent artefact first described by Lennox et al.[49–51]. This can be accounted for by adding the additional high impedance circuits represented in yellow in Scheme 1 and further depicted in SI. Very large impedances are involved in those additional elements, so that they do not influence the behavior and fits in the high frequency region. They are better evidenced in the range 0.1-100 Hz (Figure S3-S6) that could be explored in this potential range. This behavior at low frequencies also explains the poor resolution of the faradaic peaks observed at low scan rates (*i.e.* 10 Vs^{-1}, see Figure S1). The equivalent circuit is potential dependent and simplifies to a single resistance R_{surf} at $E \sim E^0$. Otherwise, we note that the value of C_{DL} (0.731 nF at -0.150 V *vs* Pt polarization) is in agreement with the one that can be assessed though with less precision by cyclic voltammetry (0.75 nF at -0.150 V vs Pt on the CV at 2000 Vs^{-1}). It will not be discussed further below and we focus now onto the high frequency range (10^2–10^7 Hz).

When *E* gets closer to E^0 (blue dots in Figure 3, see also Figures S7-S14), the phase shift transition occurs at lower frequencies, in agreement with apparition of the additional capacitance C_{ads}. Impedance data were then analyzed in the framework presented above. In Figures 3a-d (green line), a single $R_{CT}C_{ads}$ circuit is added. A discrepancy is observed in the Bode plot and emphasized in the *C*" fits. Therefore, we progressively added other $R_{CTi}C_{adsi}$ elements to include faster and slower electron transfers as suggested by Creager et al. and displayed in Scheme 1.[44] The progressive improvement of the fit is presented in SI and in Figure 3. For 4 components, an excellent fit is obtained (see Scheme 1). The calculated k_{ETi}^0 and corresponding Γ_i^0 for one and four components are given in Table 1. In all fits, we note that φ ≥ 0.890 for expected C_{DL} and C_{ads} capacitances, so that the proposed electrical equivalent schemes are physically relevant.

Table 1. Values of kinetic parameters k_{ETi}^0 and corresponding molecular coverages Γ_i^0 obtained at $E = E^0$. Fits for impedance spectroscopy and simulation parameters used for reconstruction for cyclic voltammetry with 1 and 4 populations.

	Impedance		Cyclic voltammetry	
	k_{ETi}^0 (s^{-1})	Γ_i^0 ($nmol.m^{-2}$)	k_{ETi}^0 (s^{-1})	Γ_i^0 ($nmol.m^{-2}$)
1 population	68700 ± 2000	80 ± 3	65000	75
4 populations	3900 ± 200	17 ± 1	4000	13
	22600 ± 1000	19 ± 2	25000	30
	95800 ± 3000	28 ± 1	80000	23
	390000 ± 15000	17 ± 1	400000	9

Similarly, we analyzed further the oxidation and reduction peaks of the CVs at 4 different scan rates by incorporating 4 different rate constants. The results are presented in Figure 4 and Table 1 for 20000 Vs^{-1} and in Figures S15-18 for lower scan rates. A very accurate reconstruction of both waves is observed, and the obtained values for rate constants and surface coverages are comparable to those obtained with impedance, confirming that the dispersion indeed originates from a distribution of kinetic rate constants, probably due to slightly different adsorption configurations onto the gold electrode.

In our previous study, we analyzed the kinetics for different coverages and found that electron transfer was faster for less dense monolayers. All k_{ET}^0 were however found in the range 1.7-5.8x10^5 s^{-1} whereas coverages were larger. The discrepancy is thus significant. Albeit there is no apparent influence of counter ion limitation, previous experiments were performed with tetraethylammonium tetrafluoroborate instead of tetrabutylamonium hexafluorophosphate that was used here. One possibility is that PF_6^- and BF_4^- contribute in the global reorganization energy and thus may influence k_{ET}^0. We suggest alternatively that in the present case, the contributions from

different populations are modified when electrode preparation, adsorption time and rinsing procedures are different. Surface roughness may also play a role that will be scrutinized in the future. This is probably involved by changes in the average distance between redox centers and the electrode. In the complex assemblies presented by the rotaxane, there are indeed many degrees of freedom. The ring may translate onto the axle, and the anchor is very flexible. Overall, the precise conformation of the adsorbed molecule is unknown and thus the distance between the ferrocene entities and the electrode, which regulates the electronic coupling and finally k_{ET}^0. For future integration of these giant supramolecular structures in devices, it will be essential to further tailor their interaction with the electrode to impose a single conformation.

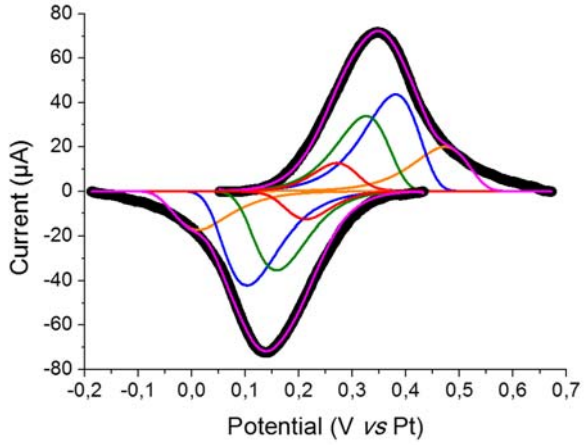

Figure 4. Reconstruction of the CV oxidation and reduction peaks at 20000 Vs^{-1} taking into account 4 populations. Γ_i^0 and k_{ETi}^0 values are given in Table 1.

Conclusion

In this contribution, we demonstrated that impedance measurements performed in a large frequency range are complementary to voltammetric ones for investigating fast electron transfer within a complex supramolecular system. We showed with our combined approach that for the complex molecule **1**, the kinetic behavior is complex and that a distribution of different populations with different rate constants on the electrode surface should be considered. We expect in the future to push further the methodology and include the interactions and possible recognition and conformation changes in the analysis.[20,52,53] In the example examined therein, CV and impedance data were consistent, but we expect that this may not be the case in the future for other systems, for example those that display molecular movements. The results obtained on molecule **1** inform that even if flexibility of molecular devices may be an advantage compared to those used in conventional electronics, this may also introduce kinetic dispersions deleterious for practical applications. Solving these issues may be addressed either by appropriate molecular design or by the development of new surface preparation procedures.

Experimental Section

Electrode preparation and modification

Gold ball ultramicroelectrodes were made by sealing a 30µm gold wire inside a glass pipet. About 100 µm of the wire protruded and was them melted in a butane flame. The electrode area was estimated by performing cyclic voltammetry in a ferrocene solution as described by Compton et al.[54] Prior to each experiment the gold surface was cleaned by applying 3 cycles in the range -0.60 to 1.20 V *vs* Pt in a 0.50 M H_2SO_4 solution. The electrode surface was then reconstructed by flame annealing. We observed that this procedure provided the best reproducibility. Molecule **1** was then adsorbed onto the electrode by immersion into a 10 µM solution of **1** in dichloromethane for at least 40 h in a fridge. Then, the electrode was rinsed and transferred in pure dichloromethane for 30 mins to remove any physisorbed molecule. The electrode was then directly transferred to the electrolyte solution.

Electrochemical measurements

For each electrode, all CV and impedance measurements were performed the same day in acetonitrile (VWR) + 0.50 M tetrabutylammonium hexafluorophosphate (Alfa Aesar, 98%) as supporting electrolyte. A platinum wire was used as counter electrode, and another platinum wire was used as a reference electrode. We indeed observed artefacts in the measurements at high frequencies with a classical Saturated Calomel Electrode (SCE) as often observed.[55] The Pt reference was calibrated versus SCE prior each experiment (E_{Pt} = 0.203 V *vs* E_{SCE}). Impedance measurements were performed with an Autolab potentiostat equipped with the ECI10M module that allows impedance acquisitions up to 10 MHz. Prior each impedance spectrum acquisition, a control CV at 2000 Vs^{-1} was performed to check the SAM integrity. 6 frequencies per decade with an excitation amplitude of 10 mV were first acquired in the range 0.1 Hz–10 MHz for 3 DC potentials below E^0. Then, the same procedure was applied at 3 potentials E close to E^0 but in the range 10 Hz-10 MHz to avoid degrading the SAM at low frequencies. The validity of impedance measurements was verified with Kramers-Krönig relations. Deviations at frequencies larger than 1 MHz are ascribed to limitations of the potentiostat. Fast scan measurements were performed in the range 10 – 40000 Vs^{-1} with a home-made potentiostat allowing ohmic drop compensation.[56] All experiments were performed at room temperature (293 K).

Data analysis

Simulations of CVs were performed with a home-made Matlab program (Butler-Volmer) or with the Digielch® software (Marcus). For impedance data fitting and simulations, we used the 1.0.4 version of the Matlab (R2019a) program ZfitGUI developed by Jean-Luc Dellis (Laboratoire de la Physique de la Matière Condensée, UFR des Sciences, Amiens, France).[57] Mathematica® was used for establishing analytical expressions given in the supplementary information.

Acknowledgements

This worked was founded by Sorbonne Université, the CNRS and Agence Nationale de la Recherche (grant FastGiant ANR-17-CE07-0012-01).

Keywords: cyclic voltammetry • impedance • self-assembled monolayers • rotaxane • electron transfer

References

[1] J.-M. Savéant, C. Costentin, *Elements of Molecular and Biomolecular Electrochemistry: An Electrochemical Approach to Electron Transfer Chemistry 2nd edition*, Wiley, Hoboken, NJ, **2019**.
[2] R. G. Nuzzo, D. L. Allara, *J. Am. Chem. Soc.* **1983**, *105*, 4481–4483.
[3] D. K. Schwartz, *Annu. Rev. Phys. Chem.* **2001**, *52*, 107–137.
[4] H. O. Finklea, in *Encycl. Anal. Chem.* (Ed.: R.A. Meyers), Wiley, Chichester, UK, **2006**, p. a5315.
[5] L. L. Rouhana, M. D. Moussallem, J. B. Schlenoff, *J Am Chem Soc* **2011**, *133*, 16080–16091.
[6] C. D. Bain, E. B. Troughton, Y. T. Tao, J. Evall, G. M. Whitesides, R. G. Nuzzo, *J. Am. Chem. Soc.* **1989**, *111*, 321–335.
[7] E. Laviron, *J. Electroanal. Chem.* **1979**, *101*, 19–28.
[8] E. Laviron, *J. Electroanal. Chem. Int. Electrochem.* **1979**, *100*, 263–270.
[9] E. Laviron, *J. Electroanal. Chem. Int. Electrochem.* **1974**, *52*, 395–402.
[10] C. Smith, H. White, *Anal. Chem.* **1992**, *64*, 2398–2405.
[11] O. Alévêque, E. Levillain, *Electrochem. Commun.* **2015**, *51*, 137–143.
[12] O. Alévêque, E. Levillain, *Electrochem. Commun.* **2016**, *67*, 73–79.
[13] O. Alévêque, E. Levillain, *Electrochem. Commun.* **2013**, *34*, 165–169.
[14] O. Alévêque, E. Levillain, Y. Morille, *J. Electroanal. Chem.* **2020**, *873*, 114414.
[15] O. Alévêque, P.-Y. Blanchard, C. Gautier, M. Dias, T. Breton, E. Levillain, *Electrochem. Commun.* **2010**, *12*, 1462–1466.
[16] A. Kiani, M. A. Alpuche-Aviles, P. K. Eggers, M. Jones, J. J. Gooding, M. N. Paddon-Row, A. J. Bard, *Langmuir* **2008**, *24*, 2841–2849.
[17] C. Amatore, E. Maisonhaute, B. Schöllhorn, J. Wadhawan, *ChemPhysChem* **2007**, *8*, 1321–1329.
[18] W. J. Albery, P. N. Bartlett, C. P. Wilde, J. R. Darwent, *J. Am. Chem. Soc.* **1985**, *107*, 1854–1858.
[19] G. K. Rowe, M. T. Carter, J. N. Richardson, R. W. Murray, *Langmuir* **1995**, *11*, 1797–1806.
[20] T. M. N. Trinh, I. Nierengarten, H. Ben Aziza, E. Meichsner, M. Holler, M. Chesse, R. Abidi, C. Bijani, Y. Coppel, E. Maisonhaute, B. Delavaux-Nicot, J.-F. Nierengarten, *Chem. Eur. J.* **2017**, *23*, 11011–11021.
[21] A. Coskun, M. Banaszak, R. D. Astumian, J. F. Stoddart, B. A. Grzybowski, *Chem. Soc. Rev.* **2012**, *41*, 19–30.
[22] J. E. M. Lewis, M. Galli, S. M. Goldup, *Chem. Commun.* **2017**, *53*, 298–312.
[23] J.-P. Collin, C. Dietrich-Buchecker, P. Gaviña, M. C. Jimenez-Molero, J.-P. Sauvage, *Acc. Chem. Res.* **2001**, *34*, 477–487.
[24] S. F. M. van Dongen, S. Cantekin, J. A. A. W. Elemans, A. E. Rowan, R. J. M. Nolte, *Chem. Soc. Rev.* **2014**, *43*, 99–122.
[25] C. J. Bruns, J. F. Stoddart, *Acc. Chem. Res.* **2014**, *47*, 2186–2199.
[26] C. Amatore, E. Maisonhaute, G. Simonneau, *J. Electroanal. Chem.* **2000**, *486*, 141–155.
[27] X.-S. Zhou, B.-W. Mao, C. Amatore, R. G. Compton, J.-L. Marignier, M. Mostafavi, J.-F. Nierengarten, E. Maisonhaute, *Chem. Commun.* **2016**, *52*, 251–263.
[28] A. J. Bard, L. R. Faulkner, *Electrochemical Methods: Fundamentals and Applications 2nd edition*, Wiley, New York, **2001**.
[29] A. Baranski, T. Krogulec, L. Nelson, P. Norouzi, *Anal. Chem.* **1998**, *70*, 2895–2901.
[30] P. Fortgang, E. Maisonhaute, C. Amatore, B. Delavaux-Nicot, J. Iehl, J.-F. Nierengarten, *Angew. Chem. Int. Ed.* **2011**, *50*, 2364–2367.
[31] C. Amatore, Y. Bouret, E. Maisonhaute, J. Goldsmith, H. Abruna, *Chem. Eur. J.* **2001**, *7*, 2206–2226.
[32] C. Amatore, E. Maisonhaute, *Anal. Chem.* **2005**, *77*, 303A-311A.
[33] M. Steffenhagen, A. Latus, T. M. N. Trinh, I. Nierengarten, I. T. Lucas, S. Joiret, J. Landoulsi, B. Delavaux-Nicot, J.-F. Nierengarten, E. Maisonhaute, *Chem. Eur. J.* **2018**, *24*, 1701–1708.
[34] C. E. D. Chidsey, *Science* **1991**, *251*, 919–922.
[35] M. C. Henstridge, E. Laborda, N. V. Rees, R. G. Compton, *Electrochimica Acta* **2012**, *84*, 12–20.
[36] K. Weber, S. E. Creager, *Anal. Chem.* **1994**, *66*, 3164–3172.
[37] L. Tender, M. T. Carter, R. W. Murray, *Anal. Chem.* **1994**, *66*, 3173–3181.
[38] L. A. Hockett, S. E. Creager, *Langmuir* **1995**, *11*, 2318–2321.
[39] S. E. Creager, G. K. Rowe, *J. Electroanal. Chem.* **1997**, *420*, 291–299.
[40] M. E. Orazem, B. Tribollet, *Electrochemical Impedance Spectroscopy*, Wiley, Hoboken, NJ, **2017**.
[41] D. Garreau, J. Saveant, D. Tessier, *J. Electroanal. Chem.* **1979**, *103*, 321–333.
[42] D. Garreau, J. Saveant, D. Tessier, *J. Phys. Chem.* **1979**, *83*, 3003–3007.
[43] S. E. Creager, T. T. Wooster, *Anal. Chem.* **1998**, *70*, 4257–4263.
[44] J. Li, K. Schuler, S. E. Creager, *J. Electrochem. Soc.* **2000**, *147*, 4584.
[45] F. G. Davia, S. E. Herrera, E. J. Calvo, *J. Phys. Chem. C* **2019**, *123*, 13939–13943.
[46] P. R. Bueno, G. Mizzon, J. J. Davis, *J. Phys. Chem. B* **2012**, *116*, 8822–8829.
[47] P. R. Bueno, F. Fabregat-Santiago, J. J. Davis, *Anal. Chem.* **2013**, *85*, 411–417.
[48] P. R. Bueno, T. A. Benites, M. S. Góes, J. J. Davis, *Anal. Chem.* **2013**, *85*, 10920–10926.
[49] E. Boubour, R. B. Lennox, *Langmuir* **2000**, *16*, 4222–4228.
[50] E. Boubour, R. B. Lennox, *Langmuir* **2000**, *16*, 7464–7470.
[51] E. Boubour, R. B. Lennox, *J. Phys. Chem. B* **2000**, *104*, 9004–9010.
[52] B. Delavaux-Nicot, H. Ben Aziza, I. Nierengarten, T. M. N. Trinh, E. Meichsner, M. Chesse, M. Holler, R. Abidi, E. Maisonhaute, J.-F. Nierengarten, *Chem. Eur. J.* **2018**, *24*, 133–140.
[53] C. Amatore, D. Genovese, E. Maisonhaute, N. Raouafi, B. Schoellhorn, *Angew. Chem. Int. Ed.* **2008**, *47*, 5211–5214.
[54] Y. Wang, E. I. Rogers, R. G. Compton, *J. Electroanal. Chem.* **2010**, *648*, 15–19.
[55] A.-T. Tran, F. Huet, K. Ngo, P. Rousseau, *Electrochimica Acta* **2011**.
[56] C. Amatore, C. Lefrou, F. Pfluger, *J. Electroanal. Chem.* **1989**, *270*, 43–59.
[57] J.-L. Dellis, Laboratoire De La Physique De La Matière Condensée, UFR Des Sciences, Amiens, France, **2020**. https://www.mathworks.com/matlabcentral/fileexchange/69811-zfitgui

Entry for the Table of Contents

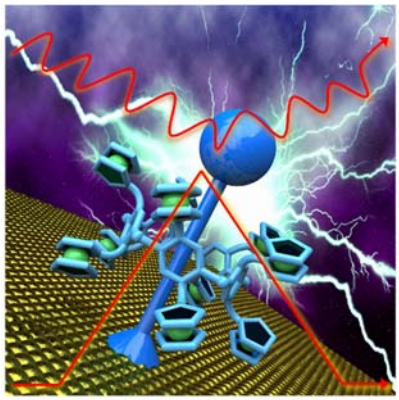

Fast scan cyclic voltammetry and high frequency electrochemical impedance spectroscopy are very complementary methods to analyze electron transfer processes in an electroactive giant rotaxane.